Pulse-front tilt for short-wavelength lasing by means of traveling-wave plasma-excitation

Davide Bleiner* and Thomas Feurer

Institute of Applied Physics, University of Bern, Sidlerstrasse 5, Bern CH-3012, Switzerland

*Corresponding author: bleiner@iap.unibe.ch

Received 25 September 2012; accepted 2 November 2012;
posted 12 November 2012 (Doc. ID 176907); published 20 December 2012

Generation of coherent short-wavelength radiation across a plasma column is dramatically improved under traveling-wave excitation (TWE). The latter is optimized when its propagation is close to the speed of light, which implies small-angle target-irradiation. Yet, short-wavelength lasing needs large irradiation angles in order to increase the optical penetration of the pump into the plasma core. Pulse-front back-tilt is considered to overcome such trade-off. In fact, the TWE speed depends on the pulse-front slope (envelope of amplitude), whereas the optical penetration depth depends on the wave-front slope (envelope of phase). Pulse-front tilt by means of compressor misalignment was found effective only if coupled with a high-magnification front-end imaging/focusing component. It is concluded that speed matching should be accomplished with minimal compressor misalignment and maximal imaging magnification.

OCIS codes: 070.0070, 140.0140, 320.0320, 050.0050.

1. Introduction

High-power laser irradiation of matter generates hot and dense plasmas. Among the various applications, laser-produced plasmas are used as gain media to generate a short-wavelength laser, by means of amplified spontaneous emission (ASE), which by means of seeding can enhance the coherence [1]. The ASE process is accomplished as a high-gain single-pass along a "plasma column" that must remain hot and dense as long as the propagating ASE front is growing till saturation. Normal incidence irradiation (the angle is here defined between the target surface and the beam) leads to multiple counter propagating ASE trajectories across the entire volume of the plasma column [Fig. 1(a)]. This splits the output between both plasma column endings, and causes degradation of the beam collimation, due to the spread in trajectories within the output aperture. A further difficulty for single-shot normal incidence pumping is related to the plasma lifetime. In fact, a longer plasma column demands increasingly more pump energy, such that the plasma remains in a hot and dense quasi-steady state (know as QSS) for the entire ASE propagation [2].

A turnaround to the limitations described was introduced with transient collisional excitation [3,4], i.e., using multiple short pulses, and in particular with so-called *traveling-wave excitation* (TWE). Here the pump beam is inclined to the target [Fig. 1(c)], such that the pump irradiates the target with a certain temporal spread between the pulse-front's leading and trailing edge. In fact, the leading edge induces the plasma a few tens of picoseconds in advance to the trailing edge, for a plasma column of 10–15 mm. The cascaded pulse-front deposition produces a propagating "plasma surge" that preserves its hot and dense conditions throughout, regardless the column length. Further, the TWE propagation efficiently bunches the gain toward one of the plasma column endings. For a given irradiation angle ϑ, the nominal TWE speed is obtained as a vectorial projection of the speed of light along the plasma column, i.e., $v_{\mathrm{TWE}} = c/\cos\vartheta$. Ideally, the v_{TWE} must remain close to the speed of light such that the "plasma surge" and the ASE front propagate in superposition, and feedback is thus maximized.

1559-128X/12/368848-06$15.00/0

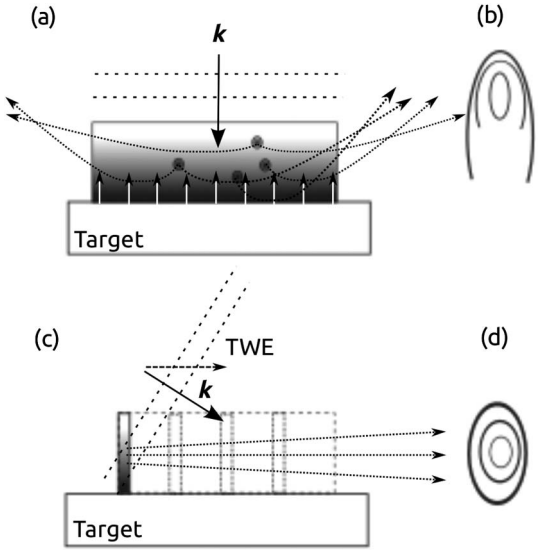

Fig. 1. Schematic of the laser-produced plasma column generation. In (a) normal incidence irradiation is shown, such that a plasma column develops "hot spots" from which beamlets amplify in a refractive medium. In (b) beam profile is visualized. In (c) TWE scheme is shown, which homogenizes the profile (d) of the output short-wavelength beam.

However, such a speed matching condition is obtained for small irradiation angles of $\vartheta < 25°$, considering as high as 10% deviation from $v_{\mathrm{TWE}} \approx 1c$.

On the other hand, for shorter wavelengths amplification the pump pulse must be deposited deeper into the plasma, where higher electron density is found to collisionally pump higher energy states. Upon penetration across the inhomogeneous plasma medium, the pump pulse refracts away because the plasma refractive index is smaller than 1. The *turning-point* plasma density (n_{TP}), attained by pump penetration into the plasma, is calculated as $n_{\mathrm{TP}} = n_c \sin^2 \vartheta$, where n_c is the plasma critical density. Henceforth, for small irradiation angles the pump meets its turning point already at a small fraction of the critical density. For cutting down the ASE wavelength one must thus choose large irradiation angles, in order to get as close as possible to the dense high collisional-pumping region. The latter requirement of *large* irradiation angle poses a *trade-off* with TWE close to $1c$ that requires a *small* angle.

In this paper, we investigate a technique to overcome such trade-off, by means of decoupling the TWE speed versus turning-point dependency. This is essential to permit efficient plasma-based lasing below the $\lambda = 10$ nm limit in laboratory-scale installations. The basic idea integrates with existing components of a common pump systems for realizing ASE lasing. In fact, in chirped-pulse amplification (CPA) a stretched pulse is amplified and then recompressed using a grating pair (compressor) [5–9]. The two compressor gratings must be perfectly parallel to achieve optimum recompression over the entire beam diameter. If the two gratings are not parallel aligned, a residual angular dispersion "leaks out" in the propagating "compressed" pulse. Angular dispersion causes a tilting of the pulse front. Indeed, in our approach the grating pair was intentionally misaligned, in order to tailor a controlled amount of pulse-front *back*-tilt, and with that compensate the TWE increase at larger ϑ (Fig. 2). In fact, the TWE depends on the pulse-front slope (envelope of amplitude), whereas the optical penetration depends on the wavefront slope (envelope of phase). Differently from the literature [10], we present a direct attempt of pulse-front tilt using the CPA setup already implemented in the pump setup, thus avoiding introducing additional components for *ad-hoc* pulse-front tilt, which may degrade throughput.

Aim of this work was thus to evaluate quantitatively the possibility of pulse *back*-tilt at large irradiation angle, in order to match the TWE speed to c. A one-dimensional (1D) Fourier optics code was written for computing the parametric dependence between the compressor misalignment and the pulse characteristics. Experimental data on the pulse structure and TWE speed were used for benchmarking.

2. Fourier Optics Model

Fourier optics considers, within the paraxial approximation, a set of superposed plane waves in order to obtain the natural modes of the propagation medium itself [11], i.e., the E field characteristics over space ($k_{x,y}$) and time. Specific transfer functions are deployed to compute the evolution of the electric field across a certain "optical element." The latter can be a lens, mirror, or grating, but also free space. Combination of multiple elements in an optical setup are handled with the product of the individual transfer functions.

The pulse coming from the stretcher into the compressor was modelled as a Gaussian beam with the following relation:

$$E_{\mathrm{stret}}(k,\omega) = \left(\frac{1}{w_o}\right) \exp\left[-\frac{1}{4}(k_x \cdot w_o)^2\right] \times \exp\left[(\omega-\omega_o)\left(\frac{1}{4}\frac{1}{\Delta\omega}\right)^2\right] \times \exp\left[-i\frac{\phi_2}{2}(\omega-\omega_o)^2\right]. \quad (1)$$

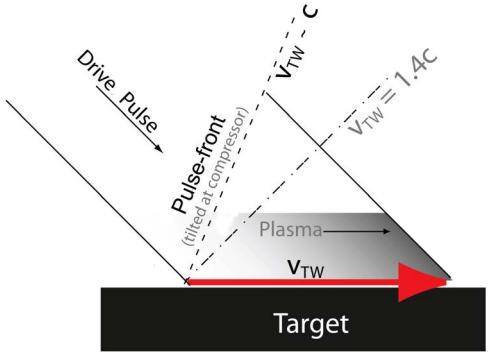

Fig. 2. (Color online) Schematic of the pulse-front back-tilt technique to match the ASE speed with the propagation speed of the plasma traveling-wave at large angle of irradiation (here 45°).

The first term of Eq. (1) is the axially symmetric spatial profile with Gaussian distribution in the wave vector domain. The second term is the frequency distribution, around the central frequency ω_o. The third term is the pulse chirp.

Figure 3 sketches out the unfolded two-grating structure of the compressor as a four-grating compressor, i.e., showing grating elements (G_1 till G_4) symmetrically centred about a roof folding mirror (M). In line of principle, both the four-grating system of Fig. 3 and our experimental system with two-grating in double-pass optical geometry are possible. The differences are in the factor of 2 footprint and in the fact that in the two-grating folded design a tilt of the second grating is consistently produced in the fourth grating as well, by means of the symmetry condition. At the front-end, the imaging/focusing element (F) is shown, which reduces the pump beam to a 10–15 mm line focus.

To begin with, the free-space propagation (FSP) transfer function is expressed as follows, with propagation in the z axis:

$$E_{\mathrm{FSP}}(k_x,\Omega) = E_o(k_x,\Omega)\exp\left[-ikz - \frac{iz}{2k}k_x^2\right], \quad (2)$$

where the FSP is applied on the input field E_o. A pulse impinging on a grating is then recomputed with the grating-dispersion (GD) transfer function, which is expressed as follows:

$$E_{\mathrm{GD}}(k_r,\Omega) = \frac{1}{b}E_o\left(\frac{k_r+\gamma\Omega}{b},\Omega\right), \quad (3)$$

where $b = \cos\alpha/\cos\beta_o$ is the beam-width change upon diffraction, where α is the angle of incidence on the grating, β_o is the angle of diffraction for the central frequency, $\gamma = (2\pi M)/(\omega_o G\cos\beta_o)$ is the coupling through the linearized grating equation, with M the diffraction order and G the grating constant, and $\Omega = \omega - \omega_o$ is the relative frequency with respect to the central frequency ω_o.

In a CPA compressor, the pulses are transformed by FSP and GD such that the emerging field is computed by combination of the Eqs. (2) and (3) as much as the experimental setup requires (Fig. 3). In the context of our double-pass compressor, a four-grating system with symmetry about a folding mirror, gives the following field *amplitude* after the last compressor grating (indices refer to the specific element number as in the illustration):

$$\begin{aligned} E_{\mathrm{comp}}(k_r,\Omega) = {} & \frac{1}{b_1b_2b_3b_4}\times E_o\left(\frac{1}{b_1b_2}\left(\frac{1}{b_3b_4}(k_x-\gamma_4\Omega+b_4\gamma_3\Omega)-\gamma_2\Omega+b_2\gamma_1\Omega\right),\Omega\right) \\ & \times\exp\left[-\frac{i\Delta}{2k}\left[\left(\frac{k_x-\gamma_4\Omega+b_4\gamma_3\Omega}{b_2b_3b_4}-\frac{\gamma_2\Omega}{b_2}\right)^2+\left(\frac{k_x-\gamma_4\Omega}{b_4}\right)^2\right]\right] \\ & \times\exp\left[-\frac{id}{k}\left(\frac{k_x-\gamma_4\Omega+b_4\gamma_3\Omega}{b_3b_4}\right)^2\right]\times\exp[-2ik(d+\Delta)]. \end{aligned} \quad (4)$$

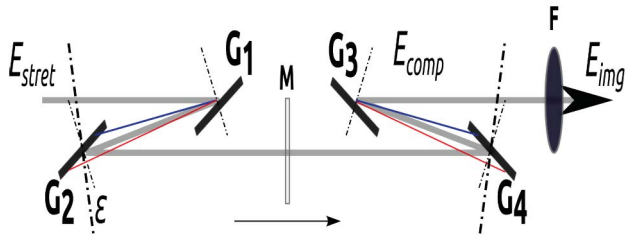

Fig. 3. (Color online) Schematic of the compressor setup for the 1D Fourier optics computation. G is indicating the gratings, M is the folding mirror, F is the imaging optics, ε is the G_2 tilt angle.

The spectral *phase* of the propagating pulse can be expressed as a Taylor series, as follows:

$$\phi(\Omega) = \phi_o + \phi_1\Omega + \phi_2\frac{\Omega^2}{2} + \phi_3\frac{\Omega^3}{6} + \ldots \quad (5)$$

The second-order phase term (*chirp*) of a grating compressor is obtained from Eq. (4) as follows:

$$\phi_2 = -\frac{i\Delta}{k}\gamma_1^2\Omega^2, \quad (6)$$

which for the present case provided values of $-1.02\cdot 10^4$ (Ti:sapphire) and $-3.11\cdot 10^2$ (Nd:glass). An analytical expression has been reported in the literature [12] as follows:

$$\phi_2 = \frac{\lambda_o}{2\pi c^2}\left(\frac{\lambda_o}{G}\right)^2\frac{L}{\cos^3\beta_o}\Omega^2, \quad (7)$$

with the orthogonal grating separation L. Equation (7) provides values in perfect agreement with the result obtained by means of Fourier optics in Eq. (6).

Finally, the compressed pulse is imaged on the target by means of focusing optics [13]. The target is some distance away from the last grating and the transfer function of an imaging/focusing component with the focal length f is as follows:

$$E_{\mathrm{img}}(r,\Omega) = E_{\mathrm{comp}}(x,\Omega)\exp\left[\frac{ik}{2f}r^2\right]. \quad (8)$$

The computations were performed for the two most popular pump laser systems, namely the Nd:glass with a wavelength of 1054 ± 2 nm (i.e., carrier

wavelength and bandwidth) and for a Ti:sapphire laser with a wavelength of 800 ± 10 nm. The Gaussian beam waist radius was $w_o = 66$ mm and focused using a $f = 609.6$ mm spherical mirror under an irradiance angle (defined between the target and the beam) of 48°. The compressor had gratings with $G^{-1} = 1740$ lpmm, and the chirped pulse stretch per bandwidth was 296 ps/nm, as in our experimental setup. The roof mirror had a half-distance $d = 1360$ mm. The angle of incidence of the stretched pulse on the first grating was 60.8°. The imaging system had a magnification of 5∶1 ($m = 0.2$).

3. Results and Discussion

The characteristics of the compressed pulse were computed as a function of grating misalignment. It was critical to quantify benefits of misalignment, i.e., the pulse back-tilt, versus the drawback, i.e., the pulse broadening. Pulse broadening causes loss of peak irradiance (power per unit surface). Variable irradiance as a function of beam radius leads to a transversely inhomogeneous plasma column in temperature and density. We begin discussing quantitatively how much peak power loss is generated at the uncompressed pulse boundary in an Nd:glass or Ti:sapphire pump. Figure 4 summarizes the relative pulse broadening as a function of grating tilt. The uncompressed pulse duration is normalized to the computed Fourier-limited pulse duration at the centerline (point of best compression), i.e., $\tau_o = 0.82$ ps (Nd:glass), $\tau_o = 0.09$ ps (Ti:sapphire). It is noted that short wavelength and small bandwidth mitigate the broadening effect, and in the present case the best compromise is provided by the Nd:glass laser. Ideally, one would like this dependence to be moderate, in order to prevent drastic changes in pulse peak power across the beam diameter. The quantification of this effect was done for a normalized pulse energy and considering the effective pulse duration in picoseconds at the pulse boundary, which is the point of worst recompression, in an Nd:glass and Ti:sapphire pump. Figure 5 shows the ratio of the latter versus the former laser system as a function of grating tilt. One notes that the ratio increases and plateaus at approximately factor of 2, indicating that pulse broadening in an uncompressed Ti:sapphire causes as twice as much peak power deterioration than in an Nd:glass. The fact that the trend levels off indicates that the chosen range of study for the tilt is reasonable to provide complete overview on the parametric change.

Concerning the effective control on the pulse-front slope, Fig. 6 summarizes the pulse tilt as a function of second compressor grating tilt. Ideally, one would like the sensitivity to be moderate, in order to facilitate the task of compressor alignment with larger tolerance. However, for the purpose of TWE velocity matching, it would be desirable to achieve a remarkable sensitivity between pulse-front tilt and grating misalignment. One notes that the calculated dependence is a function of laser system, with the Nd:glass showing a more remarkable influence. This is in agreement with what is discussed in Pretzler *et al.*

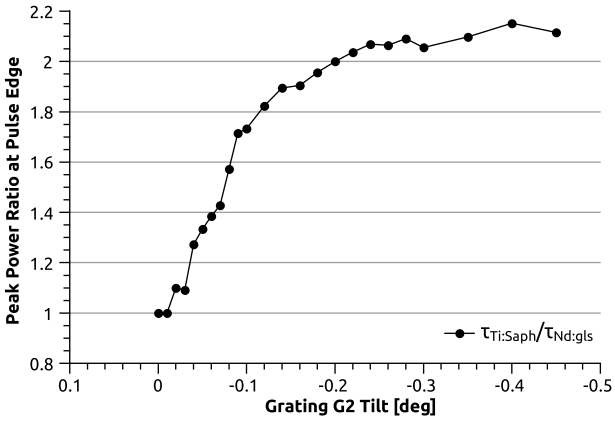

Fig. 5. Ratio of peak power in a uncompressed Ti:sapphire versus Nd:glass pulse as a function of compressor misalignment.

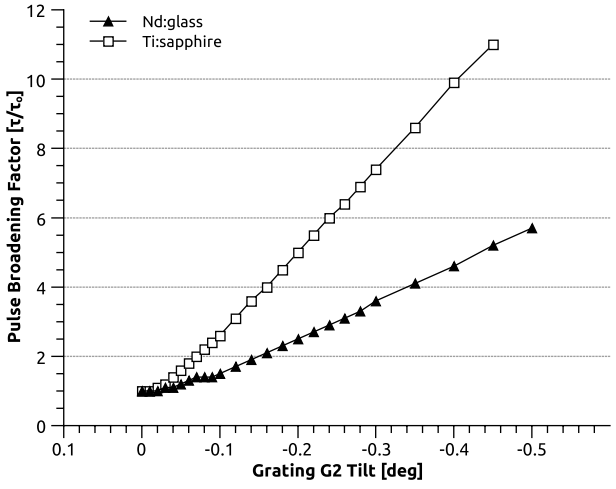

Fig. 4. Pulse broadening at the beam boundary as a function of compressor misalignment.

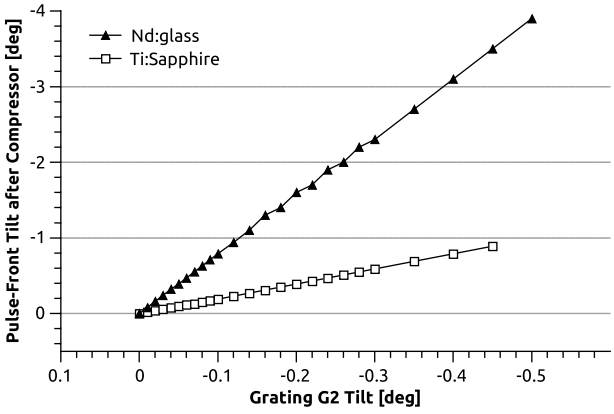

Fig. 6. Pulse-front back-tilt right after the compressor (E_{comp} in Fig. 3) as a function of compressor misalignment, and for a selection of laser pumps.

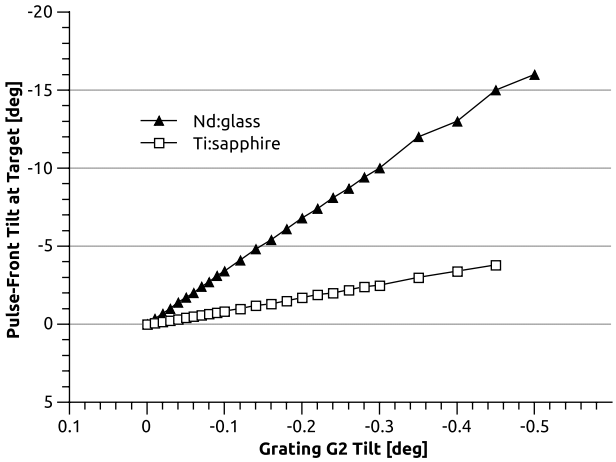

Fig. 7. Pulse-front back-tilt at the target (E_{img} in Fig. 3) as a function of compressor misalignment, and for a selection of laser pumps.

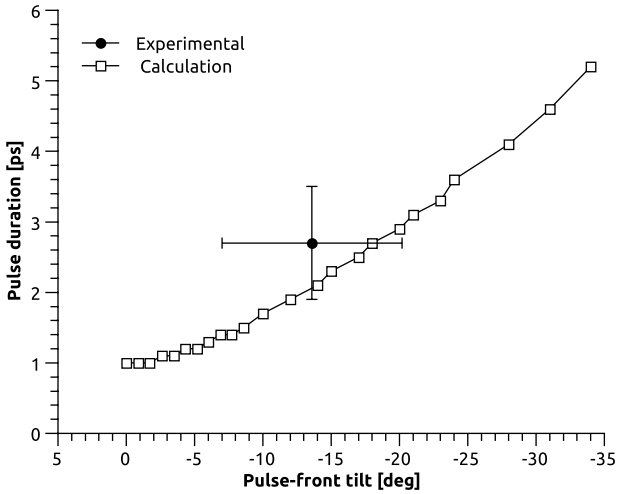

Fig. 9. Pulse-front tilt after the misaligned compressor versus concomitant pulse uncompression.

[7] that showed that the pulse tilt was a linear function of the angular chirp times the wavelength. This indicates that a better TWE velocity matching at large irradiation angle is achieved with the Nd:glass laser pump.

Figure 7 indicates that substantial pulse back-tilt is mostly achieved through the imaging element, proportionally to the magnification, when compared with Fig. 6. In fact, for a given beam width, a shorter line focus means a steeper back-tilt of the pulse-front. This drastically enhances the pulse-tilt that was possible to induce after the compressor (Fig. 6). Therefore, it is concluded that TWE velocity matching should be accomplished with minimal compressor misalignment and maximal imaging magnification. The misalignment of the compressor in fact causes concomitant degradation of the pulse compression, as shown above (Fig. 4).

Finally, the combined effect on the TWE speed is shown, as a function of compressor misalignment, in Fig. 8. The nominal TWE speed at irradiation angle 48° is $1.5c$ but for a compressor grating tilt of −0.5° a reduction of TWE speed down to $1.2c$ is computed for the $\lambda = 1054$ nm pump (Nd:glass).

The University of Bern ASE laser, which uses a Nd:glass pump, was used for experimental benchmarking. The system, in the current setup, has a beam of 133 mm in diameter that is focused onto the target over a line focus of 12 mm. This configuration gives an imaging ratio of 11:1 ($m = 0.09$). Figure 9 shows, for the University of Bern system, the calculated interrelation between pulse-front tilt and concomitant pulse uncompression, expressed as duration at the boundary (worst case). The experimental data are also shown. The pulse duration data were obtained using an autocorrelator. The pulse-tilt data were obtained determining the TWE speed using a streak camera connected to the leading

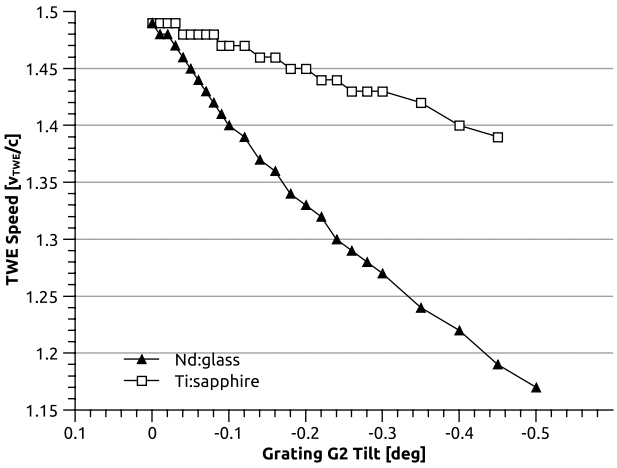

Fig. 8. Traveling-wave excitation speed along the line focus, after speed matching with compressor-grating tilt, for a irradiation angle of 48° on the target.

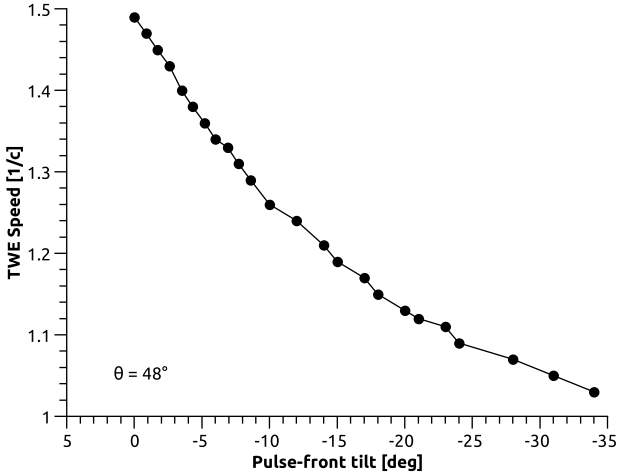

Fig. 10. TWE speed obtained with a 11-fold imaging, showing feasibility of 1c speed matching even at an angle of irradiation of 48°. For comparison, Fig. 8 shows a more modest compensation since a factor of 2 lower magnification was considered there.

and trailing edges of a line focus with optical fibers. This allowed determining the delay of pulse-font delivery at the leading and trailing edge, and thus the pulse-front slope ($\zeta = 58.6° \pm 6.6°$). Considering that for this experiment an angle of irradiation of 45° was used, the excess slope on the target ($\zeta = 13.6°$) was attributed to the compressor misalignment and imaging.

Figure 10 shows the calculated TWE speed dependency to the pulse-front tilt for the experimental 11-fold imaging setup. The result shows that with a significantly higher front-end magnification (11-fold) than what discussed in the rest of the paper (5-fold), it is possible to obtain complete TWE speed matching. This result is indeed possible for a compressor misalignment that is not dramatically degrading the pulse duration at the beam boundary, and thus preserving a reasonable transverse profile in the plasma column.

4. Conclusions

Pulse-front tilt to compensate TWE velocity at large target-irradiation angle, needed for short-wavelength lasing, was shown to be effective only if coupled with a strong front-end imaging/focusing component. The study shows that with a approximately 10-fold front-end magnification it is possible to obtain *complete* TWE speed matching, for less than half degree compressor-grating tilt. The alternative technique of using large compressor tilting and modest imaging magnification is negatively affecting the performance. Indeed, concomitant pulse broadening at the beam boundary can be very large, depending on wavelength and bandwidth. Variable irradiance as a function of beam radius, consequence of transverse pulse broadening, leads to a transversely inhomogeneous plasma column in temperature and density. It is noted that short wavelength and small bandwidth mitigate the broadening effect, and in the present case the best compromise is provided by the Nd:glass laser.

The present work was supported by the Swiss National Science Foundation under the grant number PP00P2-133564/1. Support from F. Staub, J. E. Balmer, Ch. Imesch is acknowledged.

References

1. Ph. Zeitoun, G. Faivre, S. Sebban, T. Mocek, A. Hallou, M. Fajardo, D. Aubert, Ph. Balcou, F. Burgy, D. Douillet, S. Kazamias, G. de Lachze-Murel, T. Lefrou, S. le Pape, P. Mercdji, H. Merdji, A. S. Morlens, J. P. Rousseau, and C. Valentin, "A high-intensity highly coherent soft x-ray femtosecond laser seeded by a high harmonic beam," Nature **431**, 426–429 (2004).
2. J. Dunn, A. I. Osterheld, L. Yuelin, J. Nilsen, and V. N. Shlyaptsev, "Transient collisional excitation x-ray lasers with 1-ps tabletop drivers," IEEE Sel. Top. Quantum Electron. **5**, 1441–1446 (1999).
3. A. Klisnick, D. Ros, P. Zeitoun, A. Carillon, P. Fourcade, S. Hubert, G. Jamelot, C. L. S. Lewis, A. Mac Phee, R. O'Rourcke, R. Keenan, P. Nickles, K. Janulewicz, M. Kalashnikov, J. Warwick, J. C. Chanteloup, A. Migus, E. Salmon, C. Sauteret, and J. P. Zou, "Transient pumping of Ni-like Ag with a sub-ps pump pulse in a travelling-wave geometry,"J. Opt. Soc. Am. B **17**, 1093–1097 (2000).
4. P. V. Nickles, V. N. Shlyaptsev, M. Kalachnikov, M. Schnuerer, I. Will, and W. Sandner, "Short pulse x-Ray laser at 32.6 nm based on transient gain in Ne-like titanium," Phys. Rev. Lett. **78**, 2748–2751 (1997).
5. D. Strickland and G. Mourou, "Compression of amplified chirped optical pulses," Opt. Commun. **55**, 447–449 (1985).
6. C. Fiorini, C. Sauteret, C. Rouyer, N. Blanchot, S. Seznec, and A. Migus, "Temporal aberrations due to misalignments of a stretcher-compressor system and compensation," IEEE J. Quantum Electron. **30**, 1662–1670 (1994).
7. G. Pretzler, A. Kasper, and K. J. Witte, "Angular chirp and tilted light pulses in CPA lasers," Appl. Phys. B **70**, 1–9 (2000).
8. J. C. Chanteloup, E. Salmon, C. Sauteret, A. Migus, Ph. Zeitoun, A. Klisnick, M. Carillon, S. Hubert, D. Ros, P. Nickles, and M. Kalachnikov, "Pulse-front control of 15-TW pulses with a tilted compressor, and application to the subpicosend traveling-wave pumping of a soft-x-ray laser," J. Opt. Soc. Am. B **17**, 151–157 (2000).
9. S. Akturk, X. Gu, E. Zeek, and R. Trebino, "Pulse-front tilt caused by spatial and temporal chirp," Opt. Express **12**, 4399–4410 (2004).
10. J. A. Fulop and J. Hebling, "Applications of tilted-pulse-front excitation," in *Recent Optical and Photonic Technologies*, K. Y. Kim, ed. (InTech, 2010).
11. J. W. Goodman, *Introduction to Fourier Optics* (Roberts & Co., 2004).
12. J. C. Diels and W. Rudolph, *Ultrashort Laser Pulse Phenomena* (Elsevier, 2006).
13. D. Bleiner, J. E. Balmer, and F. Staub, "Line focusing for soft x-ray laser-plasma lasing," Appl. Opt. **50**, 6689–6696 (2011).